Time-resolved diffuse optical tomography system based on compressive measurements

Andrea Farina, Marta Betcke, Laura Di Sieno, Andrea Bassi, Nicolas Ducros, Antonio Pifferi, Gianluca Valentini, Simon Arridge, Cosimo d'Andrea

Time-resolved diffuse optical tomography system based on compressive measurements

ANDREA FARINA[1,*], MARTA BETCKE[2], LAURA DI SIENO[3], ANDREA BASSI[3], NICOLAS DUCROS[4], ANTONIO PIFFERI[3], GIANLUCA VALENTINI[1,3], SIMON ARRIDGE[2], AND COSIMO D'ANDREA[1,3,5]

[1] *Consiglio Nazionale delle Ricerche, Istituto di Fotonica e Nanotecnologie, Piazza L. da Vinci 32, 20133 Milano, Italy*
[2] *Centre for Medical Image Computing, University College London, Malet Place, London WC1E 6BT, United Kingdom*
[3] *Politecnico di Milano, Dipartimento di Fisica, Piazza L. da Vinci 32, 20133 Milano, Italy*
[4] *University of Lyon, INSA-Lyon, Université Lyon 1,CNRS, Inserm, CREATIS UMR 5220 U1206, F-69621, Villeurbanne, France*
[5] *Center for Nano Science and Technology@PoliMi, Istituto Italiano di Tecnologia, I-20133 Milan, Italy*
[*] *Corresponding author: andrea.farina@polimi.it*

Compiled April 28, 2016

Compressive sensing is a powerful tool to efficiently acquire and recontruct an image even in Diffuse Optical Tomography (DOT) applications. In this work a time-resolved DOT system based on structured light illumination, compressive detection and multiple views acquisition has been proposed and experimentally validated on a biological tissue-mimicking phantom. The experimental scheme is based on two Digital Micromirror Devices (DMD) for illumination and detection modulation, in combination with a time-resolved single element detector. We fully validated the method and demonstrated both imaging and tomographic capability of the system, providing a state of the art reconstruction quality.

OCIS codes: *(170.6960) Tomography; (110.0113) Imaging through turbid media; (170.6920) Time-resolved imaging*

In the last decade the possibility to quantitatively reconstruct absorbing, scattering and fluorescent inclusions within *in vivo* organisms has attracted a great interest for diagnostic purposes (e.g. tumor detection)[1], functional studies (e.g. brain oximetry)[2] and molecular imaging on small animals (e.g. pharmacological research)[3]. The general measurement scheme consists of illuminating the sample and detecting the diffused light exiting from it. Then, by solving the inverse problem, based on a model of photon propagation through the biological tissue, the optical parameters in each point of the sample can be quantitatively reconstructed. It is usually referred to these modalities as Diffuse Optical Tomography (DOT) and Fluorescence Molecular Tomography (FMT) when the absorption/scattering or fluorescence properties are reconstructed, respectively.

DOT/FMT performance is mainly characterized by its capability to resolve the position and shape of inhomogeneities inside the tissue, and, consequently, improving the quantification capability of their optical parameters. Previous studies have demonstrated the importance of a dense source/detector [4] and multiple views measurement scheme [5, 6] in order to increase the tomographic spatial resolution. Moreover, further data, such as spectral and temporal information, are crucial [7, 8]. Temporal information provides three main advantages: i) better disentanglement of absorption/scattering properties; ii) temporal encoding of photons depth; iii) fluorescence lifetime quantification in the case of FMT. Spectral information (i.e. different excitation/detection wavelength) allows one to discriminate among tissue chromophores. Hence, DOT/FMT turns out to be a highly multidimensional problem with the drawback to generate a huge data set. This represents a practical limitation of these techniques because of the extremely long acquisition and computational times, which are not typically compatible with clinical and pre-clinical needs. Hence, a reduction of the acquired data set by preserving the spatial resolution, or more generally the data set information content, is highly desirable.

Following this concept, different studies have recently exploited the fact that a highly scattering medium (such as biological tissue) behaves as a low pass filter in the spatial domain. Hence, few illumination patterns, instead of the more typical raster scanning approach, can be adopted without losing significant spatial information [8–10]. This in turn leads to a reduction of the data set dimension and, consequently, of the acquisition and computational time. Recent studies have exploited such approach both in imaging and tomographic schemes and detection is generally carried out by a parallel detector such as CCD, CMOS or gated cameras [11]. Moreover, the use of a wide field approach (such as the case of structured illumination) allows one to illuminate the sample with high power without exceeding light density safety limits. This improves the signal-to-noise ratio.

Recently a patterned detection [12], following the single-pixel camera scheme [13], has been proposed for DOT/FMT applications, as well as for PhotoAcoustics [14]. Basically, the image of the diffused light exiting the sample is spatially modulated and subsequently focused on a single element detector. By repeating the measurement at different (source and/or detector) modulating patterns, the sampling is carried out in the spatial

frequency domain rather than in the case of a point detection as it is for a parallel detector or the raster scan. Due to the fact that a highly scattering medium acts as a low-pass filter in the spatial frequency domain, just few frequencies are needed.

This approach has the great advantage of exploiting the superior characteristics of a single detector (e.g higher temporal resolution and larger spectral bandwidth) and lower cost with respect to a parallel device. Moreover, comparing with raster scanning, a further advantage is the acquisition speed given by a wide field detection analogous to structured illumination approach. Finally, it is worth mentioning that both structured illumination and detection open the possibility to get images and reconstructions with increasing spatial details by increasing the number of measurements.

In this work we propose a multiple-view time-domain compressed sensing DOT system exploiting Hadamard patterns both in the illumination and collection plane, and applicable to non-planar geometries. The system has been experimentally validated on tissue phantoms with absorbing inclusions, demonstrating both imaging and tomographic capabilities.

The experimental set-up is schematically sketched in Fig. 1. The sample is illuminated by a pulsed structured light while detection is carried out either by a time-resolved Single Pixel Camera (SPC) or a Continuous Wave (CW) parallel detector. The sample is placed on a rotational stage to allow different view acquisition. By means of an acousto-optic tunable filter, light pulses at 650 nm are spectrally selected from a ps pulsed supercontinuum (rep. rate of 80 MHz) laser source (SuperK Extreme, NKT). Structured illumination is carried out by a Digital Micromirror Device (DMD Discovery kit 1100, Vialux), which spatially modulates the light, and an objective lens (f=50 cm) to create the image over an area of 3x3 cm^2 of the sample. The diffused light, exiting the sample over an area of about 2x2 cm^2, is imaged by a lens (f=60 cm) on a second DMD (DMD Discovery 4100, Vialux). A flip mirror allows us to image the DMD plane either on a low noise 16-bit cooled CCD camera (Versarray 512, Princeton Instruments) or a single element detector. The latter consists of a long working-distance objective (10X/0.25) which focuses the light reflected by the second DMD on a 1 mm diameter optical fiber. The light exiting the fiber is finally detected by a photomultiplier (PMT) (HPM-100-50, Becker & Hickl) connected to a Time-Correlated Single Photon Counting (TCSPC) board that samples the temporal profile of the diffuse light. The system is fully computer controlled by a home-made LabView software enabling an automated acquisition of the whole data set (illumination/detection patterns, sample rotation and acquisition).

The sample is a cylindrical tissue mimicking phantom (∅=20 mm, height 45 mm) made of an epoxy resin, TiO_2 (as scatterer) and toner (as absorber). By means of a time-resolved spectroscopy system [15] the optical parameters were measured: μ_a about 0.2 cm^{-1} and μ_s about 10 cm^{-1}. Two holes, drilled into the sample (∅=1.6 mm), allowed us to insert either one or two cylindrical absorbing inclusions as hereafter specified.

Initial calibration measurements are carried out, by means of the CCD camera on the detection side and of a low-cost camera on the illumination side, to localize the illumination/detection area over the sample. Then 360 shadows of the object (every 1°) have been acquired to create the mesh [6]. It is worth emphasizing that precise calibration is critical to achieving an accurate simulation of the forward problem, which in turn is a prerequisite to obtain a high quality tomographic reconstruction.

Measurements have been performed on the phantom with and without the absorbing rods. The acquisition procedure is

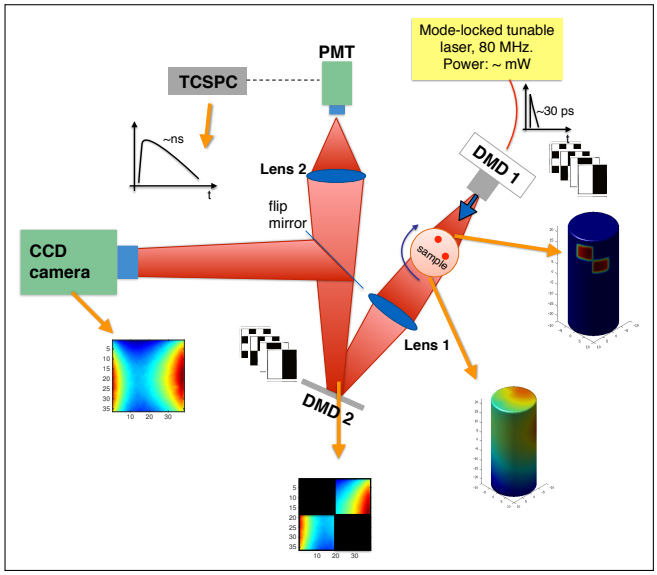

Fig. 1. Experimental set-up.

carried out by a complete 360° rotation of the sample with steps of 45° (8 views). For each view 8x8 ordered Walsh-Hadamard (WH) patterns have been used for both illumination and detection. Each WH pattern consists of two states (-1 to +1). Hence two positive patterns (ranging from 0 to +1), complementary to one another, have been acquired and properly subtracted to obtain the desired WH pattern. Acquisition time for each pattern is 1 s. A full-pixel image can be recovered by applying the fast Walsh-Hadamard inverse transform to the detected data [16].

For the reconstruction of the absorption map in the volume, the following objective function has been constructed:

$$\Psi(\mathbf{x}) = \frac{1}{2}\sum_n \left[\frac{y_n - f_n(\mathbf{x})}{f_n(\mathbf{x})}\right]^2 + \tau R(\mathbf{x}) \qquad \textbf{(1)}$$

where $\mathbf{x}$ is the absorption coefficient in every mesh element, y_n is the measurement, f_n is the forward model, τ is the hyperparameter, R is a regularization functional and n is the measurement index. The software TOAST, a finite-element based solver [17], has been used to calculate $f_n(\mathbf{x})$. In order to minimize the objective function in Eq. (1) a damped Gauss-Newton method based on a one dimensional line-search algorithm [18] has been implemented. A Total Variation (TV) regularization functional has been used. In the calculation of both the forward model and the Jacobian, the IRF has been taken into account by convolution in time.

First measurements have been carried out to demonstrate the imaging capability of the system and to estimate the number of patterns to be used in the tomographic reconstruction. In particular time-resolved data acquired by SPC have been integrated over time to obtain CW data and compared with the CCD images. An example of the images acquired by the CCD and the ones based on SPC (by spatially modulating the detection) is shown in Fig. 2. We observe a good agreement between the two images which improves by increasing the number of adopted patterns as reported in Fig. 2, where the Root Mean Square Error (RMSE) is reported as a function of the WH pattern order. In particular, we do not observe a significant improvement for WH pattern order higher than 8. Moreover, it is possible to observe that the RMSE plot for the inhomogeneous phantom

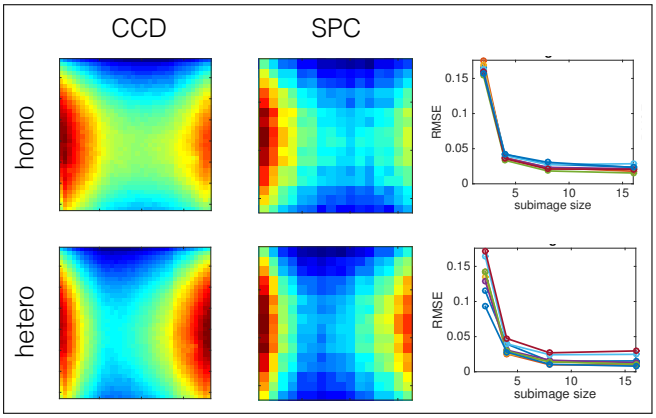

Fig. 2. Comparison between CCD and SPC images. First row: example of a CW image outcoming from the phantom without inhomogeneity measured with CCD (left) and SPC (right) using 16x16 WH patterns. The RMSE as a function of the WH order is also plotted for the eight views. Second row is analogous to the first row but the image is outcoming from the phantom with one vertical inclusion. For all the images the scale is normalized between 0 and 1.

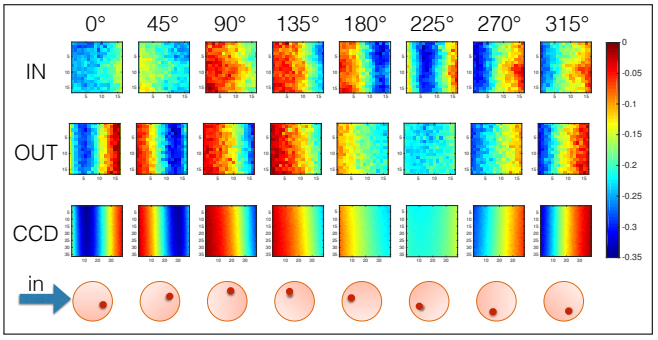

Fig. 3. Relative contrast, shown as the difference between heterogeneous and homogeneous images divided by the homogeneous one, for different rotation views (columns) in the case of spatially modulated illumination (first line), spatially modulated detection (second line) and CCD images by using uniform square illumination (third line).

presents a higher variability among the different views with respect to the homogeneous case. It is worth stressing that the number of required patterns strongly depends on the optical parameters/shape of the sample and position/dimension of the inclusions. In order to explore the imaging capability of the proposed method, the contrast provided by one inclusion, both in the CCD and SPC images, are reported in Fig. 3. In particular three cases are reported: i) the sample is illuminated with 16x16 ordered WH patterns while detection side has a uniform square pattern (first line of Fig. 3); ii) the sample is illuminated with a uniform square pattern while detection side is spatially modulated by 16x16 ordered WH patterns (second line of Fig. 3); iii) CCD images by using uniform square illumination pattern are also reported (third line of Fig. 3). In all cases the relative contrast, calculated as the difference between heterogeneous and homogeneous images divided by the homogeneous one is shown for 8 different views.

The second (modulation of detection) and third (CCD) cases show good agreement, in particular the presence of the absorbing inclusion can be clearly observed when it is located, during sample rotation, closer to the detector (CCD or SPC). On the contrary, for the other views, the inclusion cannot be observed because of the scattering. In the first case (modulation of illumination) there is no correspondence between the images acquired by the CCD and SPC. In particular we observe that by spatially modulating the illumination we can better observe the presence of the inclusions for the views where the inclusion is closer to the illumination source. In fact, the SPC approach measures the integral of the signal, then the imaging capability is not influenced by the scattering events followed by photons after impinging on the inclusion as occurs for a position sensing device like the CCD [19]. These examples demonstrate the imaging capability of the proposed method and in particular the importance of the choice of the illumination/detection patterns according to the view, the sample (shape and optical parameters) and inclusions, for both imaging and reconstruction. As a first demonstration of the tomographic capability of the proposed system, a time-resolved tomographic reconstruction by using either an early or a late gate of the time-resolved profile has been carried out. For each view, illumination consists of a squared pattern, detection of 8x8 WH patterns while the temporal gate has been chosen by integrating the TR signal on an early and a late gate, respectively. Early gate has width 300 ps ranging from 1% to 80% of the intensity peak on the rising edge, while late gate width is about 860 ps ranging from 80% to 1% of the intensity peak on the falling edge. The mesh used for the forward problem has 108000 elements and 1016 temporal point spread functions (TPSF) have been generated (127 WH patterns for 8 views) and sampled in 130 temporal steps of 12 ps width. The computational time for the forward is about 25 s on a machine mounting a 2.5 GHz quad-cores Intel i7 processor and 16 Gb RAM memory. The reconstruction has been carried out on a regular grid of 57454 points covering the whole cylindrical mesh. The Jacobian has been calculated using the adjoint method [20] implemented with direct and inverse Fast-Fourier Transform (FFT) to speed-up the temporal convolution operations. On the same machine this calculation takes about 1.5 hours. By means of the homogeneous measurements, the data acquired on the inhomogeneous phantom have been scaled to match the scale of the forward TPSFs. Three Gauss-Newton iterations have been performed. We have observed that after this iteration number the reconstruction results did not change. The overall reconstruction time is about 5 hours.

Fig. 4 shows the tomographic reconstruction of the absorption coefficient at different vertical slices (b) and 3D rendering (d) for the reconstruction using the early gate. Due to the limited field-of-view of both illumination and detection only a part of the cylinder can be reconstructed (about 18 mm from the top). We observe a good reconstruction quality concerning both the localization and relative contrast of the two inclusions. Moreover in Fig. 4 (e) an example of line profile across the inclusions at one reconstructed plane (z=17 mm) is reported for both the cases of early and late gate. As expected, we observe an improvement in both the localization and shape characterization of the inclusions by using the early gate. Finally, in order to quantify the localization capability of the reconstruction, the quadratic sum of the center of mass (COM) error for each inclusion has been computed at every section:

$$\epsilon = \sqrt{\sum_i \left[(\hat{x}_i - x_i)^2 + (\hat{y}_i - y_i)^2 \right]} \qquad (2)$$

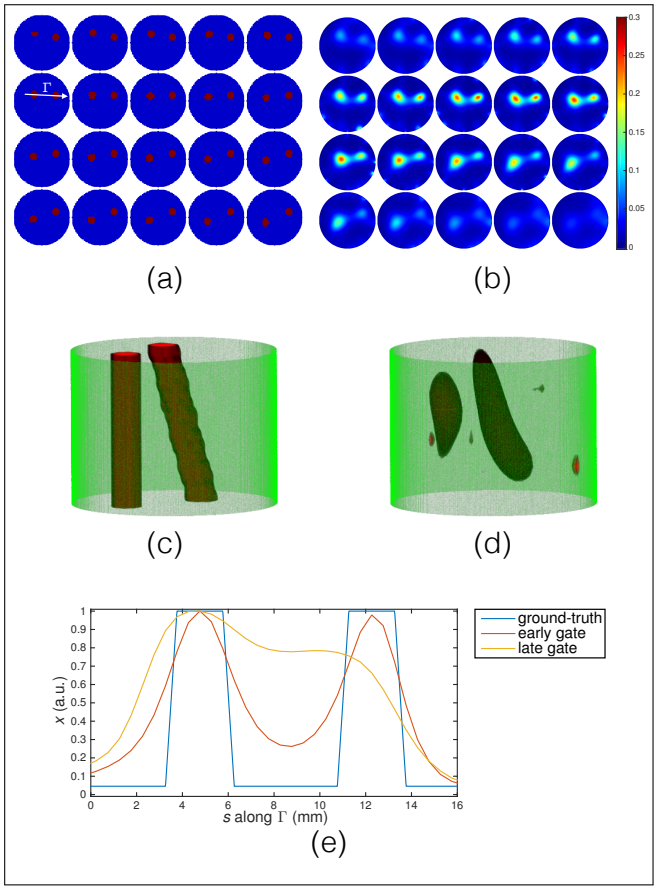

Fig. 4. Reconstruction of the absorption coefficient using an early gate. Slices are displayed from z=22.5 mm (top of the cylinder) to z=3.5 mm at step of 1 mm. The z=0 mm plane is at the middle of the cylinder; (a) ground-truth; (b) reconstruction (values are in mm^{-1}). 3D rendering: (c) ground-truth; (d) reconstructions, a threshold of one-half of the maximum absorption value has been set. (e) Profile across the line Γ connecting the two inclusion's centers on a plane at z=17.5 mm for both early (red line) and late (yellow line) gate reconstructions

.

where $(\hat{x}_i, \hat{y}_i)$ is the expected COM position at the slice i and (x_i, y_i) is the calculated COM position at the slice i. The calculation have been performed on an extended region twice larger than the inclusions. For the oblique inclusion errors of about 1.0 mm and 2.1 mm have been obtained for the early and late gate reconstruction, respectively; for the vertical inclusion we obtained 0.7 mm and 2.0 mm for early and late gate reconstruction, respectively. In conclusion, in this work, a fully tomographic time-resolved DOT system based on the sampling in the spatial frequency domain (both illumination/detection space) and multiple views acquisition has been proposed and experimentally validated on tissue-mimicking phantom, demonstrating a state of the art reconstruction quality. Moreover, the imaging capability of the system has been validated in CW by comparing SPC with a standard CCD acquisition, showing the importance of the choice of illumination/detection patterns for imaging purposes. Future work will be devoted to the optimization of the data set (choice of illumination/detection patterns, number of views and temporal gates) and system improvements (detection efficiency, calibration procedure) in order to strongly reduce the acquisition time, while preserving or even increasing the information content. In particular, adaptive basis scan approaches will be investigated [21].

This work was partially supported by Cariplo Foundation under Grant N. 2013–0615 and by the Royal Society International Exchanges 2014/R1 N. IE140259.

REFERENCES

1. D. R. Leff, O. J. Warren, L. C. Enfield, A. Gibson, T. Athanasiou, D. K. Patten, J. Hebden, G. Z. Yang, and A. Darzi, Breast Cancer Research and Treatment **108**, 9 (2008).
2. A. T. Eggebrecht, S. L. Ferradal, A. Robichaux-Viehoever, M. S. Hassanpour, H. Dehghani, A. Z. Snyder, T. Hershey, and J. P. Culver, Nature Photonics **8**, 448 (2014).
3. S. R. Cherry, Physics in medicine and biology **49**, R13 (2004).
4. S. D. Konecky, G. Y. Panasyuk, K. Lee, V. Markel, A. G. Yodh, and J. C. Schotland, Optics express **16**, 5048 (2008).
5. N. Ducros, A. Bassi, G. Valentini, M. Schweiger, S. Arridge, and C. D'Andrea, Optics letters **36**, 1377 (2011).
6. N. Ducros, A. Bassi, G. Valentini, G. Canti, S. Arridge, and C. D'Andrea, Journal of biomedical optics **18**, 20503 (2013).
7. A. Bassi, C. D'Andrea, G. Valentini, R. Cubeddu, and S. Arridge, Optics letters **33**, 2836 (2008).
8. V. Venugopal, J. Chen, F. Lesage, and X. Intes, Optics Letters **35**, 3189 (2010).
9. D. J. Cuccia, F. Bevilacqua, A. J. Durkin, and B. J. Tromberg, Optics letters **30**, 1354 (2005).
10. A. Joshi, W. Bangerth, and E. M. Sevick-Muraca, Optics Express **14**, 6516 (2006).
11. V. Venugopal and X. Intes, Journal of biomedical optics **18**, 036006 (2013).
12. Q. Pian, R. Yao, L. Zhao, and X. Intes, Optics letters **40**, 431 (2015).
13. M. Duarte, M. Davenport, D. Takhar, J. Laska, T. S. T. Sun, K. Kelly, and R. Baraniuk, IEEE Signal Processing Magazine **25** (2008).
14. N. Huynh, E. Zhang, M. Betcke, S. Arridge, P. Beard, and B. Cox, Optica **3**, 26 (2016).
15. A. Bassi, A. Farina, C. D'Andrea, A. Pifferi, G. Valentini, and R. Cubeddu, Optics Express **15**, 14482 (2007).
16. T. Beer, American Journal of Physics **49**, 466 (1981).
17. M. Schweiger and S. Arridge, Journal of biomedical optics **19**, 1 (2014).
18. M. Schweiger, S. R. Arridge, and I. Nissilä, Physics in Medicine and Biology **50**, 2365 (2005).
19. E. Tajahuerce, V. Durán, P. Clemente, E. Irles, F. Soldevila, P. Andrés, and J. Lancis, Optics Express **22**, 16945 (2014).
20. S. R. Arridge and M. Schweiger, Applied Optics (1995).
21. F. Rousset, N. Ducros, A. Farina, G. Valentini, C. D'Andrea, and F. Peyrin, "Adaptive acquisitions in biomedical optical imaging based on single pixel camera: Comparison with compressive sensing," in "13th IEEE International Symposium on Biomedical Imaging: From Nano to Macro," (2016), Proceedings 13th IEEE International Symposium on Biomedical Imaging: From Nano to Macro.

FULL REFERENCES

1. D. R. Leff, O. J. Warren, L. C. Enfield, A. Gibson, T. Athanasiou, D. K. Patten, J. Hebden, G. Z. Yang, and A. Darzi, "Diffuse optical imaging of the healthy and diseased breast: a systematic review." Breast Cancer Research and Treatment **108**, 9–22 (2008).
2. A. T. Eggebrecht, S. L. Ferradal, A. Robichaux-Viehoever, M. S. Hassanpour, H. Dehghani, A. Z. Snyder, T. Hershey, and J. P. Culver, "Mapping distributed brain function and networks with diffuse optical tomography," Nature Photonics **8**, 448–454 (2014).
3. S. R. Cherry, "In vivo molecular and genomic imaging: new challenges for imaging physics." Physics in medicine and biology **49**, R13–R48 (2004).
4. S. D. Konecky, G. Y. Panasyuk, K. Lee, V. Markel, A. G. Yodh, and J. C. Schotland, "Imaging complex structures with diffuse light." Optics express **16**, 5048–5060 (2008).
5. N. Ducros, A. Bassi, G. Valentini, M. Schweiger, S. Arridge, and C. D'Andrea, "Multiple-view fluorescence optical tomography reconstruction using compression of experimental data." Optics letters **36**, 1377–1379 (2011).
6. N. Ducros, A. Bassi, G. Valentini, G. Canti, S. Arridge, and C. D'Andrea, "Fluorescence molecular tomography of an animal model using structured light rotating view acquisition." Journal of biomedical optics **18**, 20503 (2013).
7. A. Bassi, C. D'Andrea, G. Valentini, R. Cubeddu, and S. Arridge, "Temporal propagation of spatial information in turbid media." Optics letters **33**, 2836–2838 (2008).
8. V. Venugopal, J. Chen, F. Lesage, and X. Intes, "Full-field time-resolved fluorescence tomography of small animals," Optics Letters **35**, 3189 (2010).
9. D. J. Cuccia, F. Bevilacqua, A. J. Durkin, and B. J. Tromberg, "Modulated imaging: quantitative analysis and tomography of turbid media in the spatial-frequency domain." Optics letters **30**, 1354–6 (2005).
10. A. Joshi, W. Bangerth, and E. M. Sevick-Muraca, "Non-contact fluorescence optical tomography with scanning patterned illumination," Optics Express **14**, 6516–6534 (2006).
11. V. Venugopal and X. Intes, "Adaptive wide-field optical tomography." Journal of biomedical optics **18**, 036006 (2013).
12. Q. Pian, R. Yao, L. Zhao, and X. Intes, "Hyperspectral time-resolved wide-field fluorescence molecular tomography based on structured light and single-pixel detection," Optics letters **40**, 431–4 (2015).
13. M. Duarte, M. Davenport, D. Takhar, J. Laska, T. S. T. Sun, K. Kelly, and R. Baraniuk, "Single-pixel imaging via compressive sampling," IEEE Signal Processing Magazine **25** (2008).
14. N. Huynh, E. Zhang, M. Betcke, S. Arridge, P. Beard, and B. Cox, "Single-pixel optical camera for video rate ultrasonic imaging," Optica **3**, 26 (2016).
15. A. Bassi, A. Farina, C. D'Andrea, A. Pifferi, G. Valentini, and R. Cubeddu, "Portable, large-bandwidth time-resolved system for diffuse optical spectroscopy," Optics Express **15**, 14482 (2007).
16. T. Beer, "Walsh transforms," American Journal of Physics **49**, 466 (1981).
17. M. Schweiger and S. Arridge, "The toast ++ software suite for forward and inverse modeling in optical tomography," Journal of biomedical optics **19**, 1–15 (2014).
18. M. Schweiger, S. R. Arridge, and I. Nissilä, "Gauss-newton method for image reconstruction in diffuse optical tomography," Physics in Medicine and Biology **50**, 2365–2386 (2005).
19. E. Tajahuerce, V. Durán, P. Clemente, E. Irles, F. Soldevila, P. Andrés, and J. Lancis, "Image transmission through dynamic scattering media by single-pixel photodetection," Optics Express **22**, 16945 (2014).
20. S. R. Arridge and M. Schweiger, "Part 2 : Finite-element-method calculations," Applied Optics (1995).
21. F. Rousset, N. Ducros, A. Farina, G. Valentini, C. D'Andrea, and F. Peyrin, "Adaptive acquisitions in biomedical optical imaging based on single pixel camera: Comparison with compressive sensing," in "13th IEEE International Symposium on Biomedical Imaging: From Nano to Macro," (2016), Proceedings 13th IEEE International Symposium on Biomedical Imaging: From Nano to Macro.